Polyhedron 48 (2012) 157–166

Contents lists available at SciVerse ScienceDirect

Polyhedron

journal homepage: www.elsevier.com/locate/poly

Syntheses, characterizations and biophysical studies of Cu(II) diphenylphosphate complexes: Effect of co-ligands on their biological properties

Rajdip Dey [a,1], Debalina Bhattacharya [b,1], Parimal Karmakar [b,*], Debajyoti Ghoshal [a,*]

[a] Department of Chemistry, Jadavpur University, Jadavpur, Kolkata 700 032, India
[b] Department of Life Science and Bio-technology, Jadavpur University, Jadavpur, Kolkata 700 032, India

ARTICLE INFO

Article history:
Received 2 July 2012
Accepted 28 August 2012
Available online 21 September 2012

Keywords:
Copper(II) complex
X-ray structure
Biophysical study
DNA binding
Bridging ligand

ABSTRACT

Using the same bridging ligand, diphenyl phosphate (*dpp*), and different co-ligands, 1,10-phenanthroline (*phen*)/2,2′-bipyridine (*bpy*), two structurally similar Cu(II) complexes, $[Cu(\mu\text{-}dpp)(phen)(NO_3)]_2$ (**1**) and $[Cu(\mu\text{-}dpp)(bpy)(NO_3)]_2$ (**2**), were synthesized. These complexes were characterized by single crystal X-ray diffraction as well as other physico-chemical methods. Both complexes are dinuclear in nature, but complex **1** is extended into a 3D supramolecular architecture by π–π interactions, whereas complex **2** forms a 2D supramolecular layered structure by π–π and C–H…π interactions. We further explored the DNA binding ability of these complexes by an agarose gel electrophoresis study. Although the coordination structures of these two complexes are very similar, complex **1** was found to be more effective at DNA binding. Complex **1** showed a greater cytotoxic effect on the human hepatocellular carcinoma cell line HepG2 compared to complex **2**. Moreover, complex **1** induced more *S*-phase arrest and apoptosis in HepG2 cells than complex **2**, as determined by fluorescence activated cell sorters (FACs). Thus our results indicated that changing the co-ligands in copper complexes may rendered an overall change in the supramolecular structure as well as significant variations in the biological activities.

1. Introduction

Molecules able to irreversibly modify nucleic acids have received considerable attention due to their potential applications in molecular biology as well as in drug design [1–4]. Thus, several intriguing efforts have been observed in the last two decades to study the DNA binding ability of metal complexes to facilitate the development of metal-based anticancer drugs. Metal complexes can be associated with DNA by three distinct modes, namely external binding, groove binding and intercalation. The coordinated metal complexes can bind to DNA by either covalent linkages or being intercalated within the base pairs by means of non-covalent supramolecular forces, and both may be used to destroy malignant cells. Such metallo-intercalators formed by a covalent attachment of organic intercalators to transition metal coordination complexes can interact with DNA, and consequently modulate biological activity. Metal complexes having aromatic side arms can bind to DNA by metal coordination as well as through intercalation of the attached aromatic ligand [5–11].

cis-platin, one of the most popular metal-based anticancer drugs, shows its activity by covalent linkage to DNA [12–17], but at the same time some severe side effects of this drug have been reported [18–21]. On the other hand, the energy involvements in supramolecular interactions are quite low [22–29], and thus several other interactive weak forces can also be negotiated during the modification of the structures of anticancer agents. As a result, the design of non-covalently DNA binding anticancer drugs has become important due to their lesser toxicity and target specific nature in comparison to drugs which creates covalent linkages to DNA [30–32]. Thus, continuous efforts are being made to design such non-covalent DNA intercalators using transition metals, particularly Cu(II), for their possible use as potential anticancer drugs [10,33–36].

Different complexes of Cu(II) have been extensively studied for their DNA binding ability as well as DNA cleavage activity [3,31,32,37]. Due to the redox potential value of Cu(II), it can cleave DNA both in an oxidative way [38,39] as well as in a hydrolytic way [34–36]. In addition, some Cu(II) complexes can cleave DNA upon photo-activation, which may be potentially important for their use in photodynamic therapy (PDT) [40–44]. The Cu(II) center, along with some aromatic N, N′ donor chelating ligands, e.g., 1,10-phenanthroline and 2,2′-bipyridine, have proven efficient in this regard, due to their planar character [3,31,37]. Thus the

* Corresponding authors.
E-mail addresses: pkarmakar_28@yahoo.co.in (P. Karmakar), dghoshal@chemistry.jdvu.ac.in (D. Ghoshal).
[1] Authors have made an equal contribution.

0277-5387/$ - see front matter © 2012 Elsevier Ltd. All rights reserved.
http://dx.doi.org/10.1016/j.poly.2012.08.087

composition and specific structure of such complexes are important for therapeutic purposes.

In this work, we have synthesized two complexes of Cu(II) using the 1,10-phenanthroline and 2,2′-bipyridine ligands. Along with these, we have used a phospho-diester, diphenyl phosphate, considering the well-known biological importance of these compounds [45]. Phosphate esters are present in a variety of naturally occurring substances and man-made derivatives which can be employed for several biological applications [45]. Moreover, phosphodiesters form the backbone of DNA and RNA molecules, and that is why the recognition of these types of molecules are perhaps important when associated with Cu(II) species [46].

Here we wish to report the synthesis, characterization, single crystal X-ray structure and biological activity of two compounds, $[Cu(\mu\text{-}dpp)(phen)(NO_3)]_2$ (**1**) and $[Cu(\mu\text{-}dpp)(bpy)(NO_3)]_2$ (**2**). These complexes have been synthesized with the same bridging ligand, diphenyl phosphate (*dpp*), and two different co-ligands, 1,10-phenanthroline (*phen*) and 2,2′-bipyridine (*bpy*), In both cases the compounds are dinuclear, but complex **1** is extended into a 3D supramolecular architecture by π–π interactions, whereas complex **2** forms a 2D supramolecular sheet structure by π–π and C–H…π interactions. In order to explore the biological activity of these complexes, their DNA binding abilities have been investigated using different biophysical methods and also their cytotoxic effects have been evaluated. Complex **1** is more effective than complex **2** in binding with DNA and induces a nick in the super coiled DNA. Additionally, the cytotoxic activity of complex **1** is more than that of complex **2** on human hepatocellular carcinoma cell lines HepG2 and the cytotoxicity is mediated by *S*-phase arrest and subsequent induction of apoptosis.

2. Experimental

2.1. Materials

High purity Cu(II) nitrate trihydrate, 1,10-phenanthroline (*phen*), 2,2′-bipyridine (*bpy*), diphenylphosphate (*dpp*), propidium iodide and calf thymus DNA were purchased from Aldrich Chemical Company Inc. Ethidium bromide (EtBr) and pUC19 plasmid DNA were purchased from Bangalore Genei, India. RNAse A was obtained from SRL, India and Hoechst 33258 was purchased from Polysciences, USA. All other chemicals were of AR grade. All the chemicals are used as received without further purification.

2.2. Physical measurements

Elemental analysis (carbon, hydrogen and nitrogen) were performed using a Perkin–Elmer 240C elemental analyzer. Infrared spectra (4000–400 cm^{-1}) of powder samples were taken in KBr pellets, using a Perkin–Elmer Spectrum BX-II IR spectrometer.

2.3. Syntheses of the complexes

An aqueous solution of copper(II) nitrate trihydrate (1 mmol, 0.241 g) was mixed with a methanolic solution (10 ml) of diphenyl phosphate (1 mmol, 0.250 g) with constant stirring for 15 min. After that, a methanolic solution (10 ml) of 1,10-phenanthroline (1 mmol, 0.198 g) was added to the above mixture. After stirring the mixture for 3 h, it was filtered and the filtrate was kept in a $CaCl_2$-desiccator. Deep blue single crystals suitable for X-ray diffraction analysis were obtained after 14 days (yield 78%). *Anal.* Calc. for $C_{48}H_{36}N_6O_{14}P_2Cu_2$: C, 51.94; H, 3.26; N, 7.57. Found: C, 51.92; H, 3.25; N, 7.54%.

Complex **2** was synthesized using the same procedure as that for **1** using 2,2′-bipyridine (1 mmol, 0.156 g) instead of 1,10-phenanthroline. Blue colored single crystals suitable for X-ray diffraction analysis were obtained after 20 days (yield 83%). *Anal.* Calc. for $C_{44}H_{36}N_6O_{14}P_2Cu_2$: C, 49.76; H, 3.41; N, 7.91. Found: C, 49.74; H, 3.39; N, 7.90%.

2.4. Crystallographic data collection and refinement

Suitable single crystals of **1** and **2** were mounted on a thin glass fiber with commercially available super glue. X-ray single crystal data collection of the two crystals were performed at room temperature (25 °C) using a Bruker APEX II diffractometer, equipped with a normal focus, sealed tube X-ray source with graphite monochromated Mo-Kα radiation (λ = 0.71073 Å). The data were integrated using the SAINT [47] program and the absorption corrections were made with SADABS. All the structures were solved by SHELXS-97 [48] using the Patterson method and followed by successive Fourier and difference Fourier synthesis. Full matrix least-squares refinements were performed on F^2 using SHELXL-97 [49] with anisotropic displacement parameters for all non-hydrogen atoms. All calculations were carried out using SHELXL-97, SHELXS-97, PLATON v1.15 [50], ORTEP-3v2 [51] and WinGX system Ver-1.80 [52].

2.5. Preparations of stock solutions for biophysical and biological studies

Both the copper complexes were dissolved in DMSO at a concentration of 10 mM. The stability of the complexes in DMSO was checked by comparing the electronic spectra of the complexes in the solid state as well as in DMSO (Supplementary Fig. 1). Calf thymus (CT) DNA and pUC19 plasmid DNA were dissolved separately at a concentration of 3 mg/ml stock in 10 mM citrate phosphate buffer (pH 7.4) at room temperature. Powdered EtBr and Hoechst 33258 were dissolved in double distilled water at concentrations of 10 mM and 1 mM, respectively. Stocks were stored at 4 °C in the dark and diluted freshly by double distilled water before the experiments.

2.6. Absorption spectroscopic study of plasmid DNA with the complexes

Absorption spectroscopic studies were done on a HITACHI U-2800 spectrophotometer, using pUC19 plasmid DNA (35 μg/mL) with increasing concentrations of the complexes (10–70 μM). After each addition, the DNA and complex mixtures were incubated at room temperature for 15 min and scanned from 210 to 305 nm. Each sample was scanned for a cycle number of 2, cycle time of 5 s at a scan speed of 100 nm/min. The modified Benesi–Hildebrand equation [53] was used for the determination of the ground state binding constant between pUC19 DNA and the complex. The binding constant "*K*" was determined using the following relation:

$$A_0/\Delta A = A_0/\Delta A_{max} + (A_0/\Delta A_{max}) \times 1/K \times 1/L_t$$

where $\Delta A = A_0 - A$, ΔA_{max} = maximum reduced absorbance, A_0 - = maximum absorbance of DNA (without any ligand), A = reduced absorbance of DNA (in the presence of ligand) and L_t = ligand concentration.

2.7. Fluorescence spectroscopic studies of complexes with CT DNA

Fluorescence spectroscopic studies of CT DNA (35 μg/ml) with varying concentrations of the complexes were done by using a HITACHI F3010 spectrofluorimeter. In this experiment, EtBr solution was gradually added to the said concentration of CT DNA and at each time the fluorescence pattern was scanned. The fluorescence

intensity was saturated at 100 μM concentration of EtBr. At this saturation level, the respective complexes were added gradually (up to 90 μM) until the fluorescence pattern decreased up to the starting value again. The excitation wavelength was 546 nm and the emission spectra were scanned from 550 to 640 nm, spectral response of 2 s, along with a scanning speed of 60 nm/min. The same experiment was done using Hoechst 33258 instead of EtBr. For Hoechst 33258, the excitation wavelength was 351 nm and emission spectra were scanned from 400 to 550 nm. Saturation of fluorescence intensity was observed at a concentration of 5.3 μM of Hoechst 33258 and then the complexes were added up to 170 μM.

2.8. Study of the binding activity of the complexes by agarose gel electrophoresis

pUC19 plasmid DNA (500 ng) was incubated separately with different concentrations of both complexes and the pure *phen* ligand (0.5–5 mM) separately at 37 °C for 1 h, and then the samples were run in 2% agarose gel in 1× Tris–acetate–EDTA buffer (pH 7.4) at 2 V/cm for 12 h.

2.9. Cell culture and MTT assay

Human liver carcinoma cells (HepG2) were cultured in Dulbecco's modified eagle medium (DMEM) supplemented with 10% fetal bovine serum (FBS) and 100 U/ml penicillin–streptomycin at 5% CO_2 and 37 °C. Viability of the HepG2 cells after exposure to various concentrations of the complexes and *phen* ligand were assayed by 3-(4,5-dimethylthiazol-2-yl)-2,5-diphenyltetrazolium bromide (MTT). Briefly, cells were seeded in 96 well plates at 1×10^4 cells/well and these exponentially growing cells were exposed to the complexes at concentrations of 0, 0.1, 0.2, 0.5, 1, 2.5, 5 and 10 μM for 24 and 48 h. After incubation, the cells were washed with phosphate buffer saline (PBS) twice and incubated with MTT solution (450 μg/ml) for 3–4 h at 37 °C. The resulting formazan crystals were dissolved in an MTT solubilization buffer, the absorbance was measured at 570 nm by using a Biorad microplate reader and the values were compared to the mock-treated cells.

2.10. Cell cycle analysis

About 1×10^6 cells of HepG2 were seeded in a 90 mm tissue culture plate for 24 h. The exponentially growing cells were treated separately with 1 μM complex **1** and 4 μM complex **2**. After 24 h, the cell pellets were washed with 1× PBS and fixed with chilled 80% ethanol and kept at 4 °C for overnight. Prior to staining with 50 μg/ml propidium iodide, the cells were incubated for 1 h with 100 μg/ml of DNAse free RNAse A at 37 °C. The cell cycle was analyzed with a Becton Dickinson fluorescence activated cell sorter (FACS) Calibur flow cytometer and 25 000 events were counted at each data point [54].

2.11. Apoptosis by annexin V-FITC

Exponentially growing HepG2 cells were checked for apoptosis by addition of either complex **1** or complex **2** at the dose mentioned in the previous section, and untreated HepG2 was kept as a control. Both control and test samples were incubated for 24 h. Following the incubation, the cells were washed twice with PBS. After that, the cells at a concentration of about 1×10^6 cells/ml were resuspended in 1× annexin binding buffer. Five hundred microliters of each cell suspension was added to a FACS tube (12 × 75 mm), and 2 μg/ml of annexin V-FITC and 0.5 μg/ml of propidium iodide were added to each cell suspension. Then the tubes were incubated at room temperature for 15 min in the dark. Finally, the fluorescence of cells was immediately determined by a Becton Dickinson (FACS Calibur) flow cytometer [55].

3. Results and discussion

3.1. IR spectroscopy

Both the complexes shows very similar bands in their IR spectrum due to their similar structures. Compounds **1** and **2** shows a medium intensity band at 1208 and 1200 cm^{-1} respectively, which may be assigned to the stretching frequency (ν) of the P═O bond [56]. The ν_{as} and ν_s for the P–OR bond in **1** are observed at 1018 and 918 cm^{-1}, whereas those for **2** are at 1024 and 925 cm^{-1} respectively. The three medium intensity bands present at 1466, 1361 and 1097 cm^{-1} (for complex **1**) and 1472, 1384 and 1096 cm^{-1} (for complex **2**) correspond to $\nu_{as}(NO_2)$, $\nu_s(NO_2)$ and ν(N═O) respectively [56]. Both the complexes display medium intensity bands in the range 3100–3000 cm^{-1} which corresponds to the stretching vibration of aromatic C–H groups. The next group of bands appears for both the complexes at around 1400–1600 cm^{-1}, corresponding to the stretching vibration of aromatic C═C groups [56].

3.2. Crystal structures

3.2.1. Single crystal X-ray structure of complex *1*

Complex **1** crystallizes in the triclinic centrosymmetric $P\bar{1}$ space group. Data collection, structure refinement parameters and crystallographic data for complex **1** are given in Table 1. The complex is dinuclear in nature, where the phenyl phosphate acts as a bridging ligand (Fig. 1). Here each Cu(II) center exhibits a distorted octahedral geometry with an elongated Cu–O bond [Cu1–O7 2.6255(18) Å], which is characteristic for a *Jahn Teller* distorted Cu(II) ion. The Cu(II) center is chelated by two nitrogen atoms of the 1,10-phenanthroline (N1,N2), with Cu–N distances of 2.028(15) and 2.014(18) Å (Table 2). The other four coordination sites of the metal atom are occupied by two oxygen atoms of the nitrate ligand (O5, O7), having Cu–O distances of 1.995(16) and

Table 1
Crystallographic and structural refinement parameters for complexes **1** and **2**.

	1	**2**
Formula	$C_{48}H_{36}N_6O_{14}P_2Cu_2$	$C_{44}H_{36}N_6O_{14}P_2Cu_2$
Formula weight	1109.87	1061.83
Crystal system	triclinic	monoclinic
Space group	$P\bar{1}$	$P2_1/c$
Unit cell dimensions		
a (Å)	9.7573(4)	11.182(5
b (Å)	11.0256(4)	18.720(5)
c (Å)	12.0534(4)	11.163(5)
α (°)	88.628(2)	90
β (°)	68.447(1)	101.425(5)
γ (°)	75.615(1)	90
V (Å^3)	1164.96(8)	2290.4(16)
Z	1	2
D_{calc} (g cm^{-3})	1.582	1.540
μ (mm^{-1})	1.058	1.072
F(000)	566	1084
θ_{range} (°)	1.8–27.6	1.9–27.7
Reflections collected	19 732	33 127
Unique reflections	5353	5339
Reflections (R_{int})	4954 (0.083)	4022 (0.075)
Goodness-of-fit (GOF) (F^2)	1.09	1.06
R_1 [$I > 2\sigma(I)$][a]	0.0379	0.0541
wR_2[a]	0.1073	0.1669

[a] $R_1 = \sum||F_o| - |F_c||/\sum|F_o|$, $wR_2 = [\sum(w(F_o^2 - F_c^2)^2)/\sum w(F_o^2)^2]^{1/2}$.

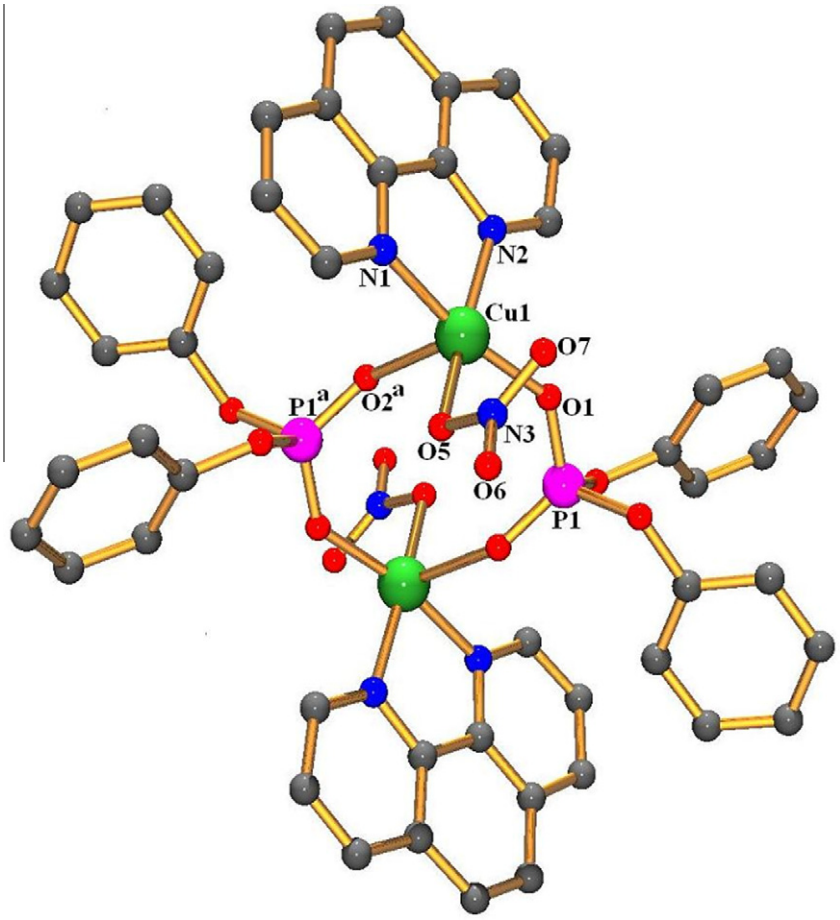

Fig. 1. Atom labeling diagram of complex **1**.

Table 2
Selected bond lengths (Å) and bond angles (°) for complex **1**.

Cu1–O1	1.9342(14)	Cu1–O5	1.9959(16)
Cu1–O7	2.6255(18)	Cu1–N1	2.0280(15)
Cu1–N2	2.0149(18)	Cu1–O2^a	2.2103(12)
O1–Cu1–O5	95.00(6)	O1–Cu1–O7	88.14(6)
O1–Cu1–N1	169.62(7)	O1–Cu1–N2	90.07(7)
O1–Cu1–O2^a	97.29(5)	O5–Cu1–O7	53.60(6)
O5–Cu1–N1	92.15(6)	O5–Cu1–N2	165.96(6)
O2^a–Cu1–O5	95.55(6)	O7–Cu1–N1	90.05(6)
O7–Cu1–N2	113.67(6)	O2^a–Cu1–O7	149.11(6)

Symmetry code: a = 1 − *x*, 2 − *y*, 1 − *z*.

2.6255(18) Å, and two O atoms from the phenyl phosphate (O1 and O2) with Cu–O distances of 1.934(14) and 2.210(12) Å (Table 2). The two nitrogen atoms (N1,N2) of the 1,10-phenanthroline and two oxygen atoms, one from the nitrate group (O5) and the other from the phenyl phosphate (O1), creates the equatorial plane. The axial sites are occupied by another oxygen atom (O2^a) of symmetry generated diphenyl phosphate (*dpp*) and the O atom (O7) from the nitrate.

In the crystal packing, two adjacent dimeric units are locked by face-to-face π–π interactions created between the aromatic rings of one *phen* moiety, which produces a one dimensional supramolecular chain along the *b* axis. In that 1D pattern, the floppy phenyl rings of *dpp* are further locked by face-to-face π–π interactions to create a supramolecular sheet structure in the *bc* plane (Fig. 2 and Table 3). Here it is interesting to note that the aromatic rings of *phen* and the phenyl rings of *dpp* are involved in π–π interactions exclusively within the rings of *phen* and *dpp* respectively. This may be attributed to the self-recognition phenomena portrayed by two different aromatic rings present in a complex. One of the aromatic rings of *phen*, which is not involved in intra-sheet π–π interactions, creates inter-sheet π–π interactions to get an overall 3D supramolecular structure (Supplementary Fig. 2 and Table 3).

3.2.2. Single crystal X-ray structure of complex *2*

Complex **2** crystallizes in the monoclinic system with the $P2_1/c$ space group. Data collection, structure refinement parameters and crystallographic data for complex **2** are given in Table 1. Like **1** this complex is also dinuclear in nature, where the phenyl phosphate acts as a bridging ligand (Fig. 3). Here also each Cu(II) center exhibits a distorted octahedral geometry with a elongated Cu–O bond [Cu1–O 2.731(4) Å] (Table 4), which is characteristic of a *Jahn Teller* distorted Cu(II) ion. Each Cu(II) is chelated by two nitrogen atoms [N1,N2; Cu–N distances 2.007(2) and 2.000(2) Å respectively] of the 2,2′-bipyridine, which along with two oxygen atoms, one from the nitrate group (O5) and the other from the diphenyl phosphate [O1^a; Cu–O distance 1.927(2) Å], create the equatorial plane of the octahedron. The axial sites are occupied by the oxygen atoms (O2) of *dpp* and the O atom (O6) of the nitrate ligand with bond distances of 2.154 (2) and 2.731(4) Å respectively (Table 4).

The crystal packing of complex **2** shows a strong face to face π–π interaction between the aromatic rings of *bpy* along the *bc* plane and the phenyl rings of the *dpp* are engaged in a C–H…π interaction with the H atom of another phenyl ring of *dpp*. These

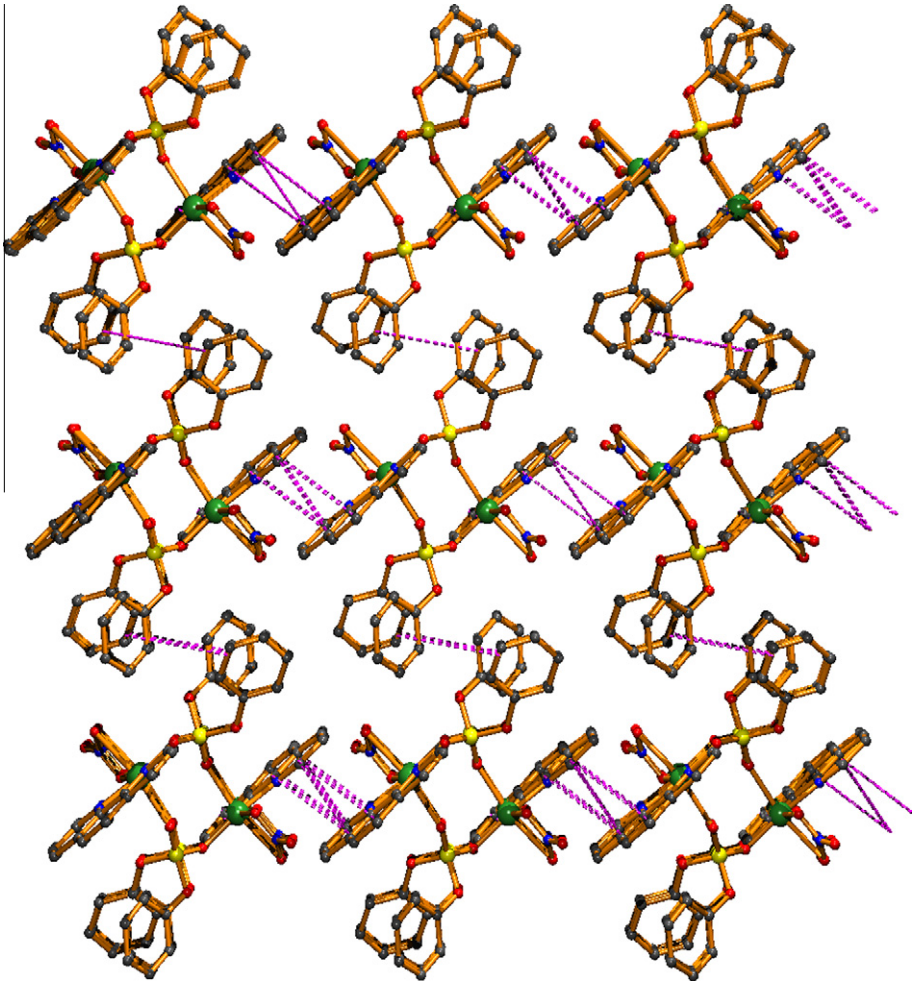

Fig. 2. Projection along *a*-axis of **1** showing the interlocking of the dimeric units.

Table 3
π–π and C–H…π interactions in **1**.

Ring(*i*) → ring(*j*)	Distance of centroid(*i*) from ring(*j*) (Å)	Dihedral angle(*i*,*j*) (°)	Distance between the (*i*,*j*) ring centroids (Å)
R(1) → R(1)^{i}	3.7657(12)	0	3.5316(8)
R(1) → R(2)^{i}	3.7227(11)	1.52(9)	3.5184(8)
R(2) → R(2)^{ii}	3.5282(11)	0	3.2752(8)
R(3) → R(1)^{i}	3.7226(11)	1.52(9)	3.5413(8)
R(4) → R(4)^{iii}	4.1829(16)	0	3.4629(11)
C–H → ring(*j*)	H…R distance (Å)	C–H…R angle (°)	C…R distance (Å)
C(14)–H(14) → R(1)^{iv}	2.98	128	3.626(2)

Symmetry code: (i) = 2 − *x*, 1 − *y*, 1 − *z*; (ii) = 2 − *x*, 2 − *y*, 1 − *z*; (iii) = −*x*, 2 − *y*, 2 − *z*; (iv) = 1 − *x*, 2 − *y*, 1 − *z*. R(*i*)/R(*j*) denotes the *i*th/*j*th rings: R(1) = N(1)/C(10)/C(9)/C(8)/C(7)/ C(11); R(2) = N(2)/C(1)/C(2)/C(3)/C(4)/ C(12); R(3) = C(4)/C(5)/C(6)/C(7)/C(11)/C(12); R(4) = C(13)/C(14)/C(15)/C(16)/C(17)/C(18).

interactions create a 2D single layer structure (Fig. 4 and Table 5). The disposition of the 2D sheets shows an almost parallel arrangement along the *b*-axis (Supplementary Fig. 3)

3.3. Bio-physical study

The *in vitro* binding of these two complexes with pUC 19 DNA was studied by absorption spectrophotometry. The absorption maxima at 258 nm of pUC 19 DNA was decreased gradually with increasing concentrations of the complexes (1.5–7.5 μM). The association

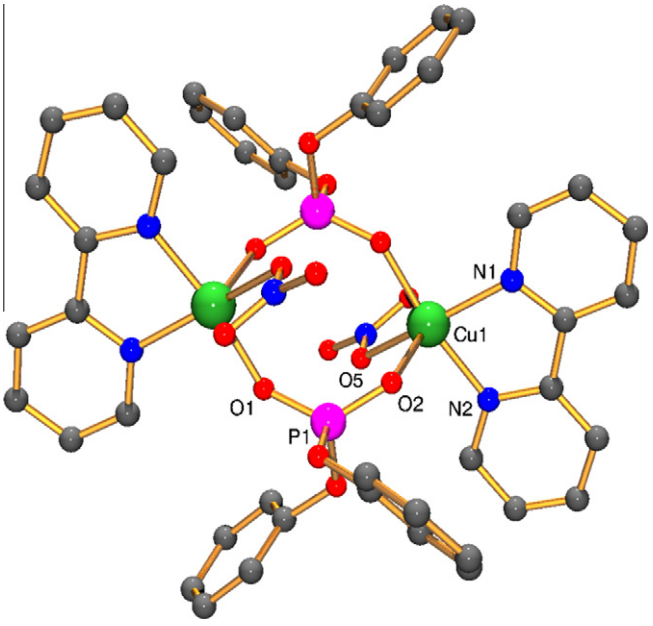

Fig. 3. Atom labeling diagram of complex **2**.

constant of complexes **1** and **2** with DNA are calculated as 3.36×10^5 and 2.7×10^5 M^{-1} respectively from the Benesi–Hilde-

Table 4
Selected bond lengths (Å) and bond angles (°) for complex **2**.

Cu1–O2	2.154(2)	Cu1–O5	2.007(2)
Cu1–O6	2.731(4)	Cu1–N1	2.007(2)
Cu1–N2	2.000(3)	Cu1–O1[a]	1.927(2)
O2–Cu1–O5	93.19(9)	O2–Cu1–O6	143.85(10)
O2–Cu1–N1	106.96(9)	O2–Cu1–N2	90.64(10)
O1[a]–Cu1–O2	93.87(9)	O5–Cu1–O6	50.65(10)
O5–Cu1–N1	159.01(9)	O5–Cu1–N2	93.51(11)
O1[a]–Cu1–O5	93.33(9)	O6–Cu1–N1	109.03(10)
O6–Cu1–N2	91.73(12)	O1[a]–Cu1–O6	88.83(10)
N1–Cu1–N2	80.74(10)	O1[a]–Cu1–N1	91.14(9)
O1[a]–Cu1–N2	171.58(10)		

Symmetry code: a = 1 − *x*, −*y*, 2 − *z*.

Table 5
π–π and C–H…π interactions in **2**.

Ring(*i*) → ring(*j*)	Distance of centroid(*i*) from ring(*j*) (Å)	Dihedral angle(*i*,*j*) (°)	Distance between the (*i*,*j*) ring centroids (Å)
R(1) → R(2)[i]	3.631(3)	2.3(2)	3.6105(19)
R(2) → R(1)[ii]	3.631(3)	2.3(2)	3.5953(16)
C–H → ring(*j*)	H…R distance (Å)	C–H…R angle (°)	C…R distance (Å)
C(15)–H(15) → R(3)[i]	2.91	149	3.739(4)

Symmetry code: (i) = *x*, 1/2 − *y*, 1/2 + *z*; (ii) = *x*, 1/2 − *y*, −1/2 + *z*. R(*i*)/R(*j*) denotes the *i*th/*j*th rings: R(1) = N(1)/C(1)/C(2)/C(3)/C(4)/C(10); R(2) = N(2)/C(8)/C(7)/C(6)/C(5)/C(9); R(3) = C(17)/C(18)/C(19)/C(20)/C(21)/C(22).

brand equation [53] (Supplementary Figs. 4 and 5). To study the ability of these compounds to interfere with the complex formed by DNA intercalated with the dye EtBr, each of the complexes was added gradually to EtBr saturated DNA and the fluorescence spectra were taken after each addition. The fluorescence intensity of pUC 19 DNA (OD 258 = 0.7) and EtBr was measured by adding increasing concentrations of EtBr (Supplementary Fig. 6). The saturation in fluorescence intensity was observed at an EtBr concentration of 100 μM, which showed maximum fluorescence intensity at an emission wavelength of 580 nm. Complex **1** was then added gradually to the EtBr saturated DNA and the fluorescence spectra were taken in each time. With the addition of complex **1**, the fluorescence intensity of EtBr saturated DNA was gradually decreased and finally returned to the basal level at a concentration of 20 μM of complex **1** (Supplementary Figs. 6a and 6b). It is important to note that neither of the complexes have any fluorescence property, either in the free form or in the DNA bounded form. Moreover, the ligand *phen* did not change the fluorescence intensity of EtBr saturated DNA (Supplementary Fig. 7). Thus, the quenching of the fluorescence intensity of EtBr saturated DNA was probably due to the binding of the complexes with DNA. When EtBr saturated DNA was challenged with increasing concentrations of complex **2**, it was seen that the fluorescence intensity slowly decreased and returned to the basal level after the addition of 80 μM solution of complex **2** (Supplementary Figs. 6c and 6d). Further, we explored the ability of the said agents to interfere with the complex formed by DNA and the DNA groove binder Hoechst 33258, a well-known DNA minor groove binder. The fluorescence intensity of a solution containing 30 μg/ml of pUC 19 plasmid DNA in 10 mM Tris–Cl [tris(hydroxymethyl)amino methane and conc. HCl] of pH 7.4 was gradually increased with the addition of increasing concentrations of Hoechst 33258. The fluorescence intensity was saturated at a concentration of 1.7 μM of Hoechst 33258 (Supplementary Fig. 8). The fluorescence intensity of the Hoechst 33258–DNA complex did not return to the basal value after gradual addition of complex **1** up to 40 μM, indicating partial displacement of the DNA groove binding dye from DNA (Supplementary Figs. 8a and 8b). It is also worth mentioning that the *phen* ligand does not change the fluorescence intensity of the Hoechst 33258–DNA complex at all (Supplementary Fig. 9). The same experiment has performed with complex **2** (Supplementary Figs. 8c and 8d), where the fluorescence intensity of the Hoechst 33258–DNA complex was slightly quenched. Thus the spectrofluorimetric data

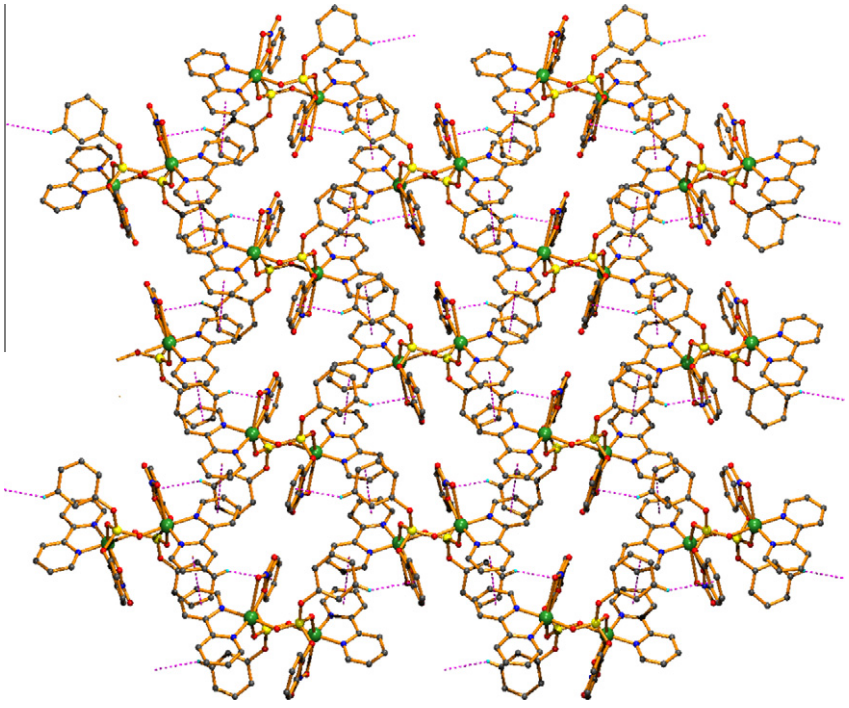

Fig. 4. 2D sheet formation in **2** along the *a*-axis by π–π and C–H…π interactions.

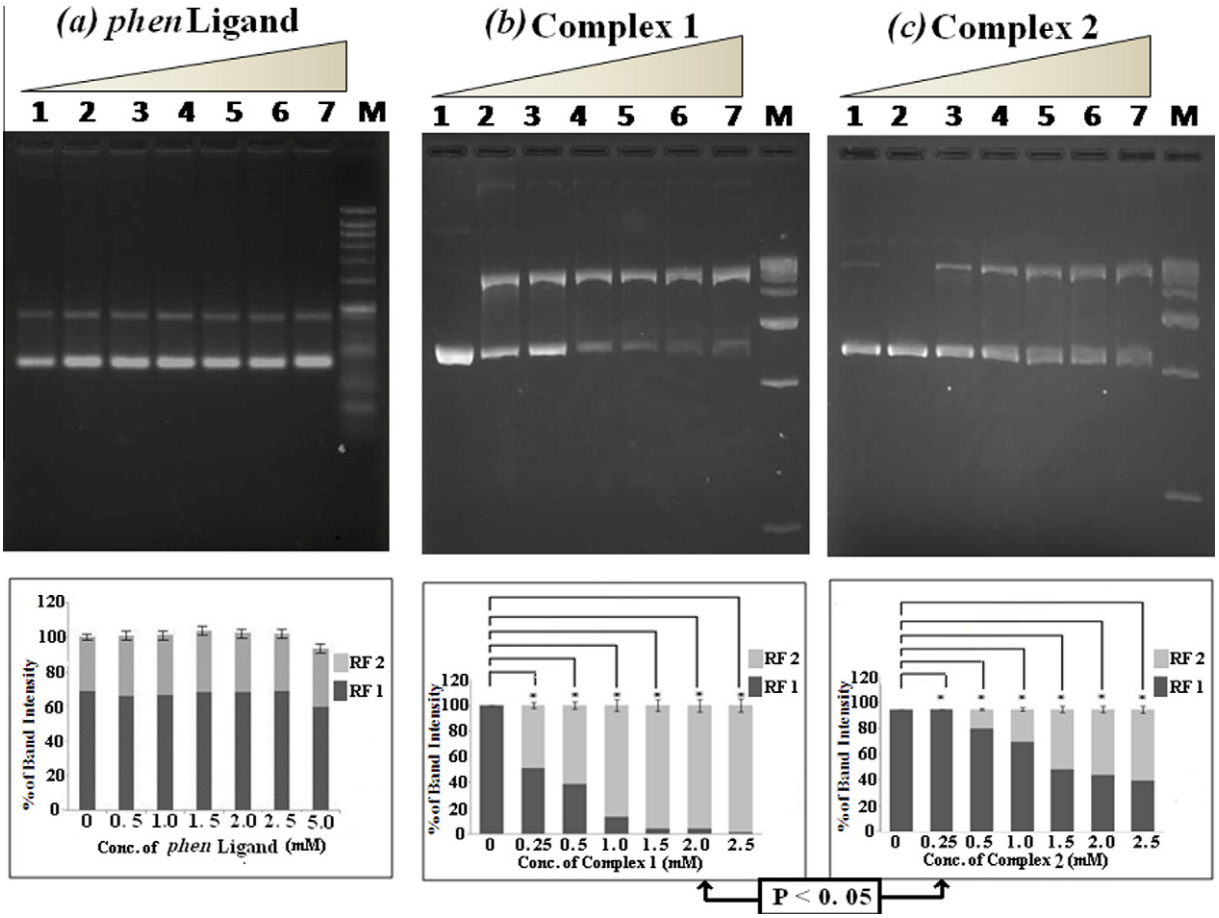

Fig. 5. Agarose gel (2%) electrophoresis study of pUC19 plasmid DNA (500 ng) with increasing concentrations of (a): ligand, (b) complex **1** and (c): complex **2**. Lane 8 is marker DNA for all figures. Relative intensity of RF1 and RF2 for respective concentrations of (a) ligand, (b) complex **1** and (c) complex **2** is plotted at the bottom.

suggest that both the complexes can interact with DNA by intercalation as well possibly having a weak partial interaction with the DNA minor groove.

3.4. Gel electrophoresis

The effect of the complexes was also studied by DNA migration in agarose gel. pUC 19 plasmid DNA was incubated for 60 min at 37 °C in the presence of increasing concentrations of the respective complexes or ligand (*phen* only), and the samples were run in 2% agarose gel in 1× TAE (a mixture of Tris base, acetic acid and EDTA) buffer of pH 7.4 at 2 V/cm for 12 h. The gel was stained with EtBr and photographs were taken in a gel documentation system. As seen in Fig. 5, the presence of *phen* did not change the DNA migration or intensity of the super coiled (RF1) DNA. But in the presence of *phen* containing complex **1**, the intensity of super coiled DNA decreased with increasing concentrations of the complex, resulting in an increased in RF2 population and indicating nicking in the plasmid DNA by complex **1**. In case of *bpy* containing complex **2**, the intensity of RF2 increased only at a higher concentration of the complex.

3.5. MTT-assay

The *in vitro* DNA binding ability of the complexes prompted us to investigate the effect of the complexes on human cell lines. Human hepatocellular carcinoma cell line HepG2 was taken and the cells were incubated in the presence of either of the complexes or *phen* for 24 h before they were subjected to an MTT assay. As seen in Fig. 6, complex **2** induces almost no effect on HepG2 cells up to 5 μM, but complex **1** shows significant cell killing ability (Fig. 6a). In order to rationalize the cell killing ability of complex **1**, we performed the same assay with the *phen* ligand only. The respective ligand induced only a moderate effect on the cells. It is interesting to note that for complex **1**, 2.5 μM is sufficient to kill all the cells. The calculated LD50 values are 1 μM for complex **1** and 2.5 μM for the free *phen* ligand.

We also tested the cytotoxic effect of the complexes, when the cells were incubated for 48 h in the presences of the complexes. Complex **2** had no effect on the HepG2 cells up to 10 μM, but complex **1** induced significant cytotoxic effects on the cells (Fig. 6b). It is evident from MTT assay that the toxic effect of complex **1** is much more than that of complex **2** and the cytotoxic effect of complex **1** is both time and concentration depended (Fig. 6). The cytotoxic effect is likely to be linked with cell cycle arrest, so we have also performed experiments on cell cycle analysis. As complex **2** was effective in killing cells at a higher concentration, we took 4 μM of complex **2** and 1 μM of complex **1**. As seen in Fig. 7, significant populations of the cells were arrested in the *S* phase when they were treated with these complexes. Complex **2** induced more *S*-phase arrest at a concentration 4 μM and complex **1** induced *S*-phase arrest at a much lower concentration (1 μM). The nature of cell death was also determined by double staining the cells with propidium iodide and annexin V-FITC. After incubation in the presence of either of the complexes for 24 h, the cells were stained simultaneously with propidium iodide and annexin V-FITC and then subjected to FACS analysis. Using same concentrations of the complexes as was used in cell cycle analysis, we found complex

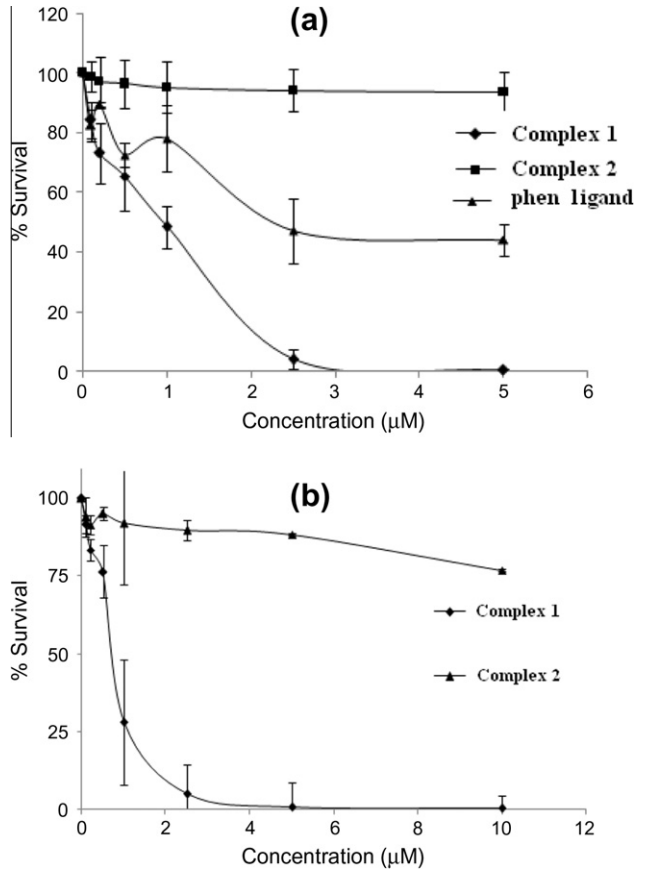

Fig. 6. Cell survivability assay. (a) HepG2 cells were incubated with increasing concentrations of the complex (**1** or **2**) or *phen* ligand for 24 h and the cells were subjected to MTT assay. (b) MTT assay done with HepG2 cells when the complexes were treated for 48 h.

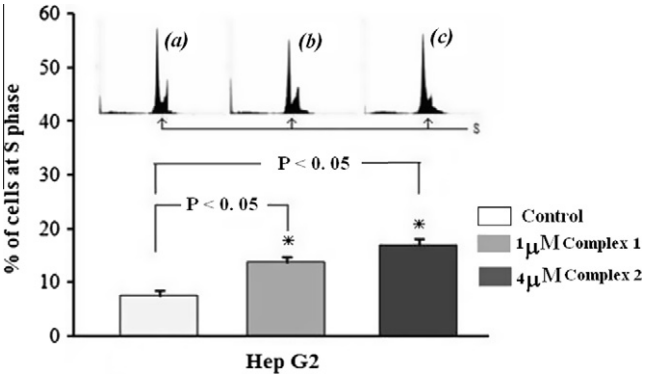

Fig. 7. Cell cycle analysis by FACS along with the statistical analysis: HepG2 cells were treated with either complex **1** or **2** for 24 h and then the cells were processed for cell cycle analysis. (a) mock treated, (b) complex **1** treated, (c) complex **2** treated. Percentage of cells in *S*-phase after treatment was plotted in the bottom panel.

1 induced 28.5% early apoptotic cells, whereas only 19.75% apoptotic cell were observed for complex **2** (Fig. 8).

3.6. Comments regarding the biophysical/biological properties

Both complexes have similar coordination structures, only with a difference with respect to the co-ligand used (*phen* and *bpy*), but during a comparison of the biophysical and biological activity we found a marked difference between the two complexes. Both the complexes bind with DNA and possibly by base intercalation or weakly through the minor groove of DNA. Apart from these methods, the complexes may bind with DNA in such a manner which distorts the DNA structure, rendering the release of EtBr or Hoechst 33258 from DNA. Both the complexes produced nicking in super coiled pUC19 DNA and consequently increased RF2 population. In the DNA migration assay it was found that complex **1** was more effective in converting supercoiled DNA into RF2 population. This might be due to the presence of the *phen* ring which can maintain planarity much better than *bpy*, and as a result complex **1** may have better chance to intercalate with DNA. Though *phen* interacts with DNA, *in vitro* it cannot produce nicking in plasmid DNA, as observed in the gel electrophoresis study. The nicking of the DNA by the complexes may be due to the presence of the transition metal. It is possible that free *phen* dissociates from the DNA or its presence may not produce any significant shift in the DNA under the gel electrophoresis conditions. Moreover, the interaction of free *phen* with DNA in cells may be responsible for the cytotoxicity of *phen* in the MTT assay.

Binding of Cu(II) to DNA and subsequent induction of single strand breaks was reported in several pieces of literature [47]. Actually it was demonstrated that copper–*phen* complexes and their conjugates are useful reagents for studying nucleic acid interactions [57]. Also, the nuclease activity of the copper–*phen* ion can be targeted to specific DNA sequences by attachment of the ligand to the 5′ end of complementary deoxyoligonucleotides via a phosphoramidate linkage [58]. Moreover, Cu(II) ions, in the presence of *phen*, O_2 and a reducing agent, degraded DNA with the release of thiobarbituric-acid-reactive material [59].

In present case, the chances for the availability of copper for interaction with DNA are poor, if not impossible. Thus the apparent activity of the complexes is due to their ligands, i.e. *bpy* or *phen*, where we clearly demonstrated that the *phen* ligand was more active than *bpy* when they were entrapped in same type of complexes. In cell survival assay it was demonstrated that *phen* containing complex **1** had a greater cytotoxic effect than *bpy* containing complex **2**. Both the complexes have the same lipophilic part (phenyl rings of phosphate), but complex **1** might effectively interfere with DNA metabolisms at much lower concentration compared to complex **2**. *In vitro* complex **1** produces a nick in the super coiled DNA, but *in vivo* it may also interfere with different cellular proteins, which are essential for replication. Also, nicking of DNA may lead the cells to arrest in the G1 or G2 rather than the *S*-phase, and the cell cycle data suggested that cells were arrested in the *S* phase after treatment with the complexes. During the *S* phase the chromosomal DNA is more accessible to the complex due to its open conformation at the sites of replication and after binding, it can induce DNA strand breaks, resulting in arrest in the *S*-phase. Additionally, complex **1** may interact with cellular proteins involved in DNA replication and thereby inducing *S*-phase arrest. Whatever the reason is, stalled DNA replication may induce genomic instability, resulting in apoptosis. In the annexin V-FITC assay, we also noticed most of the dead cells were in early apoptosis. Cell cycle arrest and subsequent induction of apoptosis is a hallmark of many DNA damaging agents. Here also, the observation that complex **1** induces apoptosis after *S*-phase arrest implicates a possible therapeutic application.

4. Conclusion

The complexes presented in this report have similar coordination structures as their compositions are similar, with the only difference being in the co-ligands *phen* and *bpy*. This difference in co-ligand makes their supramolecular arrangements different. Both

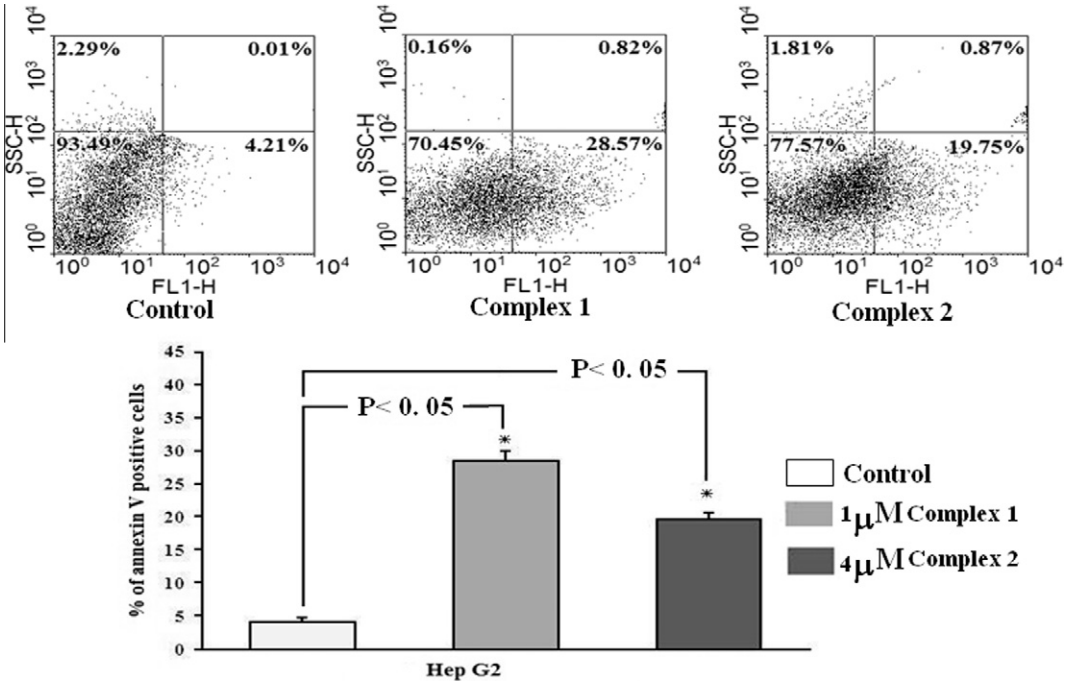

Fig. 8. Apoptosis study of HepG2 cells (24 h) by annexin V-FITC and propidium iodide staining along with the percentage of apoptotic cells after treatment in the bottom panel.

complexes can bind with DNA by displacing EtBr completely from the EtBr–DNA complex and partially displace Hoechst 33258 from the Hoechst–DNA complex. The DNA binding activity and cell killing ability of complex **1** is more effective than those of complex **2**, and the mechanism of cell killing is mediated by apoptosis. Thus it can be concluded that the slight change in co-ligand may result in the overall change in the supramolecular structure as well as the significant variation in biological properties, and thus complex **1** may have some potential implications from a therapeutic point of view. In summary, this work is a nice example of controlling structure property relationships.

Acknowledgements

The authors are gratefully acknowledged UGC for financial support under the major research scheme. The X-ray diffractometer facility under the DST FIST program is also gratefully acknowledged.

Appendix A. Supplementary data

CCDC reference numbers 859416 and 859417 contain the supplementary crystallographic data for complexes **1** and **2**. These data can be obtained free of charge via http://www.ccdc.cam.ac.uk/conts/retrieving.html, or from the Cambridge Crystallographic Data Centre, 12 Union Road, Cambridge CB2 1EZ, UK; fax: (+44) 1223-336-033; or e-mail: deposit@ccdc.cam.ac.uk. Supplementary data associated with this article can be found, in the online version, at http://dx.doi.org/10.1016/j.poly.2012.08.087.

References

[1] P.B. Dervan, Science 232 (1986) 464.
[2] M. Pitie, J.D. Van Horn, D. Brion, C.J. Burrows, B. Meunier, Bioconjugate Chem. 11 (2000) 892.
[3] D.S. Sigman, A. Mazumder, D.M. Perrin, Chem. Rev. 93 (1993) 2295.
[4] B. Meunier, DNA and RNA Cleavers and Chemotherapy of Cancer and Viral Diseases, Kluwer, Dordrecht, 1996.
[5] A. Casini, C. Gabbiani, F. Sorrentino, M.P. Rigobello, A. Bindoli, T.J. Geldbach, A. Marrone, N. Re, C.J. Hartinger, P.J. Dyson, L. Messori, J. Med. Chem. 51 (2008) 6773.
[6] A.F.A. Peacock, P.J. Sadler, Chem. Asian J. 3 (2008) 1890.
[7] Y.K. Yan, M. Melchart, A. Habtemariam, P.J. Sadler, Chem. Commun. (2005) 4764.
[8] A. Bergamo, G. Sava, Dalton Trans. (2007) 1267.
[9] H. Kopf, P. Kopf-Maier, Angew. Chem., Int. Ed. Engl. 18 (1979) 477.
[10] T.K. Goswami, B.V.S.K. Chakravarthi, M. Roy, A.A. Karande, A.R. Chakravarty, Inorg. Chem. 50 (2011) 8452.
[11] W.O. Foye, Cancer Chemotherapeutic Agents, American Chemical Society, Washington, DC, 1995.
[12] E.R. Jamieson, S. Lippard, J. Chem. Rev. 99 (1999) 2467.
[13] M. Markman, Expert Opin. Drug Saf. 2 (2003) 597.
[14] J.T. Hartmann, H.P. Lipp, Expert Opin. Pharmacother. 4 (2003) 889.
[15] T. Boulikas, M. Vougiouka, Oncol. Rep. 10 (2003) 1663.
[16] J. Reedijk, Proc. Natl. Acad. Sci. U.S.A. 100 (2003) 3611.
[17] K.R. Barnes, S. Lippard, J. Met. Ions Biol. Syst. 42 (2004) 143.
[18] T. Tanaka, K. Yukawa, N. Umesaki, Oncol. Rep. 14 (2005) 1365.
[19] S.J. Berners-Price, T.G. Appleton, in: L.R. Kelland, N. Farrell (Eds.), Platinum-based Drugs in Cancer Therapy, Humana Press, Totowa, NJ, 2000, p. 3.
[20] D. Wang, S. Lippard, J. Nat. Rev. Drug Discovery 4 (2005) 307.
[21] A.M. Angeles-Boza, P.M. Bradley, P.K.-L. Fu, S.E. Wicke, J. Bacsa, K.M. Dunbar, C. Turro, Inorg. Chem. 43 (2004) 8510.
[22] J.L. Atwood, J.E.D. Davies, D.D. MacNicol, F. Vögtle, in: J.M. Lehn (Ed.), Comprehensive Supramolecular Chemistry, Pergamon, Oxford, 1996.
[23] S. Leininger, B. Olenyuk, P. Stang, J. Chem. Rev. 100 (2000) 853.
[24] V. Balzani, L. De Cola (Eds.), Supramolecular Chemistry, Kluwer Academic, The Netherlands, 1992.
[25] M. Fujita, K. Umemoto, M. Yoshizawa, N. Fujita, T. Kusukawa, K. Biradha, Chem. Commun. (2001) 509.
[26] P. Stang, Chem. Eur. J. 4 (1998) 19.
[27] B.J. Holliday, C.A. Mirkin, Angew. Chem. Int. Ed. 40 (2001) 2022.
[28] D. Philp, J.F. Stoddart, Angew. Chem. Int. Ed. 35 (1996) 1154.
[29] M.D. Pluth, K.N. Raymond, Chem. Soc. Rev. 36 (2007) 161.
[30] P.U. Maheswari, S. Roy, H.D. Dulk, S. Barends, G.V. Wezel, B. Kozlevcar, P. Gamez, J. Reedijk, J. Am. Chem. Soc. 128 (2006) 710.
[31] D.S. Sigman, D.R. Graham, V.D. Aurora, A.M. Stern, J. Biol. Chem. 254 (1979) 12269.
[32] V. Rajendiran, R. Karthik, M. Palaniandavar, H. Stoeckli-Evans, V.S. Periasamy, M.A. Akbarsha, B.S. Srinag, H. Krishnamurthy, Inorg. Chem. 46 (2007) 8208.
[33] T.K. Goswami, M. Roy, M. Nethaji, A.R. Chakravarty, Organometallics 28 (2009) 1992.
[34] E.L. Hegg, J.N. Burstyn, Coord. Chem. Rev. 173 (1998) 133.
[35] F. Mancin, P. Scrimin, P. Tecilla, U. Tonellato, Chem. Commun. (2005) 2540.

[36] Y. An, S.D. Liu, S.Y. Deng, L.N. Ji, Z.W. Mao, J. Inorg. Biochem. 100 (2006) 1586.
[37] B.P. Hudson, J.K. Barton, J. Am. Chem. Soc. 120 (1998) 6877.
[38] D.S. Sigman, T.W. Bruce, C.L. Sutton, Acc. Chem. Res. 26 (1993) 98.
[39] W.K. Pogozelski, T.D. Tullius, Chem. Rev. 98 (1998) 1089.
[40] R. Bonnett, Chemical Aspects of Photodynamic Therapy, Gordon & Breach, London, UK, 2000.
[41] M.R. Detty, S.L. Gibson, S.J. Wagner, J. Med. Chem. 47 (2004) 3897.
[42] H. Ali, J.E. van Lier, Chem. Rev. 99 (1999) 2379.
[43] E.D. Sternberg, D. Dolphin, C. Bruckner, Tetrahedron 54 (1998) 4151.
[44] B.W. Henderson, T.M. Busch, L.A. Vaughan, N.P. Frawley, D. Babich, T.A. Sosa, J.D. Zollo, A.S. Dee, M.T. Cooper, D.A. Bellnier, W.R. Greco, A.R. Oseroff, Cancer Res. 60 (2000) 525.
[45] A.D.Q. Ferreira, A. Bino, D. Gibson, Inorg. Chem. 37 (1998) 6560.
[46] N. Lomadze, H.-J. Scheneider, T. Albelda, G.E. Espana, B. Verdejo, Org. Biomol. Chem. 4 (2006) 1755.
[47] SMART and SAINT, Bruker AXS Inc., Madison, WI, 1998.
[48] G.M. Sheldrick, SHELXS-97, Program for Solution of Crystal Structures, University of Göttingen, Germany, 1997.
[49] G.M. Sheldrick, SHELXL-97, Program for Refinement of Crystal Structures, University of Göttingen, Germany, 1997.
[50] PLATON: A.L. Spek, Acta Crystallogr., Sect. D 65 (2009) 148.
[51] ORTEP-32 for Windows: L.J. Farrugia, J. Appl. Crystallogr. 30 (1997) 565.
[52] WinGX – A Windows Program for Crystal Structure Analysis: L.J. Farrugia, J. Appl. Crystallogr. 32 (1999) 837.
[53] H.A. Benesi, J.H. Hildebrand, J. Am. Chem. Soc. 71 (1949) 2703.
[54] Y. Li, L. Sun, M. Jin, Z. Du, X. Liu, C. Guo, Y. Li, P. Huang, Z. Sun, Toxicol. In Vitro 25 (2011) 1343.
[55] S.S. Fard, J.M. Tehrani, M.M. Akhondi, M. Hashemi, A.M. Ardekani, Avicenna J. Med. Biotech. 2 (2010) 53.
[56] K. Nakamoto, Infrared and Raman Spectra of Inorganic and Coordination Compounds, fourth ed., Wiley–Interscience, New York, 1986.
[57] J.M. Gutteridge, J. Biochem. 218 (1984) 983.
[58] B.C. Bales, M. Pitié, B. Meunier, M.M. Greenberg, J. Am. Chem. Soc. 124 (2002) 9062.
[59] C.H. Chen, D.S. Sigman, Proc. Natl. Acad. Sci. U.S.A 83 (1986) 7147.